Korean J. Chem. Eng., 36(1), 146-156 (2019)
DOI: 10.1007/s11814-018-0178-6

pISSN: 0256-1115
eISSN: 1975-7220

Study of effective parameters for the polarization characterization of PEMFCs sensitivity analysis and numerical simulation

Sara Barati, Mohsen Mehdipour Ghazi†, and Behnam Khoshandam

Department of Chemical, Petroleum and Gas Engineering, Semnan University, 35131-19111, Semnan, Iran
(*Received 27 June 2018 • accepted 17 October 2018*)

Abstract−A three-dimensional model of a HT-PEMFC was simulated using Comsol Multiphysics software. Sensitivity was analyzed by using the three-level Box-Behnken experimental design. The effect of independent variables on the fuel cell performance including air and hydrogen velocity, temperature and amount of phosphoric acid doping level (PA_{dop}) on the membrane was investigated. The results showed that the PA_{dop} is the most important variable. The simulation results showed that with the increasing of the PA_{dop} from 2 to 16, the current density (at a voltage of 0.4 V) increased from 0.3 to 0.9 A/cm^2, which confirms the importance of the PA_{dop} factor on the fuel cell performance.

Keywords: Design Expert, Sensitivity Analysis, Box-Behnken, High Temperature PEM Fuel Cell

INTRODUCTION

Fuel cells are energy conversion devices that directly convert chemical energy of fuel like hydrogen and methanol into electrical energy based on an electrochemical reaction [1]. They are commonly classified by the types of electrolyte contained and operating temperature, which would bring unique advantages, limitations, and potential applications. In automobile and stationary applications, special interests have been given to proton exchange membrane fuel cells (PEMFCs) for their quick start-up [1]. Nafion membrane is an industrial standard in polymer fuel cells for use, by virtue of its high proton conductivity, chemical stability, flexibility, and high mechanical strength. However, these properties are valid only in a highly hydrous state and temperatures less than 80 °C [2]. Moreover, low operating temperature of PEMFC technology has always posed technical challenges, such as inefficient cogeneration and catalyst contamination [3]. So attempts are made to prepare PEMFC with modified constituents being capable of working at high temperatures [3,4]. Polybenzimidazole (PBI) polymer was proposed as high temperature PEMFC electrolyte [5]. Compared to Nafion ® membrane, this electrolyte shows excellent oxidative and thermal stability, good mechanical flexibility, low gas permeability and almost zero water electro-osmotic drag at elevated temperature [6]. Moreover, its proton conductivity is high with doping of a strong acid such as H_3PO_4 [7]. In addition, the type of polymer used in the fuel cell (there are other factors that affect the performance of the fuel cell) determining the mainly governing factor has always been a challenge for qualitative and quantitative studies. Lack of a simple explicit function to explain the role of each factor further reveals the difficulties associated in a fuel cell. In recent years, sensitivity analysis has widely been used to examine the response sensitivity of a model to the input parameters [8]. The designer has to define a set of experiments to extract the change of a goal function with respect to input parameters and find of the most influential factors [8]. Despite the success of sensitivity analysis on providing a correlation between the affecting parameters and the responses, the method has rarely been utilized for fuel cell applications. It is due to the cost associated with implementing the experimental tests and preparing a fuel cell membrane. Most of the previous work has examined the effect of several parameters on fuel cell performance. In each case, all parameters are kept as constants and the effect of one parameter on the performance of the fuel cell is independently evaluated. In these studies, the interactions of the parameters have not been investigated. There are few works that study the independent input parameters affecting the fuel cell performance and interactions of the parameters effect [9-12]. There are several methods of analysis such as regression analysis, scenario analysis [13], structural equation [14], neural networks [15] and Monte Carlo simulations [16] for investigating of parameter effects on the response. The simulator softwares such as Comsol Multiphysics have successfully been used to simulate the fuel cell performance and affecting factors [9,11]. Recently, the RSM method was used in theory study to determine the optimal conditions of affecting parameters [17]. In the present paper, by using Comsol Multiphysics software, a three-dimensional model for a high temperature PEMFC was developed, and the effects of four independent parameters on fuel cell performance including air and hydrogen velocity, operating temperature and amount of acid-doping on membrane were investigated. The results of the simulation were validated with experimental data and average current density was considered as the response. Response surface methodology (RSM), based on the three-level Box-Behnken design, was used to obtain the optimum conditions of the significant parameters.

MATHEMATICAL MODELING

In this section, a three-dimensional mathematical model was

†To whom correspondence should be addressed.
E-mail: mohsenmehdipour@semnan.ac.ir

developed to examine the impact of parameters affecting the high temperature PEM fuel cell performance. In this model, the following assumptions are made [18]:

- The system is operating under steady-state and isothermal condition.
- The flows are assumed to be laminar and incompressible [19].
- The porous layers, such as the catalyst layers, gas diffusion layers and membrane, all have homogeneous porous properties. Also, the porosity and permeability are accounted as constant values.
- All reactants, i.e., O_2 and H_2, are assumed to be ideal gases.

Applying the above-mentioned assumptions, the governing equation can be written as below.

1. Governing Equation

To describe momentum transfer in the region of gas flow channels, Navier, Stokes and continuity equations were used:

$$\nabla(\varepsilon\cdot\rho\cdot\vec{V}\vec{V}) = -\varepsilon\nabla P + \nabla\cdot(\varepsilon\mu\nabla\vec{V}) + S_V \tag{1a}$$

$$\nabla\cdot(\rho u) = 0$$

$$S_V = \begin{cases} -\dfrac{\mu}{\kappa}(\varepsilon)^2\vec{V} & \text{GDL} \\ -\dfrac{\mu^2}{\kappa_p}\varepsilon_m\varepsilon_{mc}\vec{V} + \dfrac{K_\varphi}{K_P}Z_f C_f F\nabla\varphi_e & \text{Catalyst layer} \\ -\dfrac{\mu^2}{\kappa_p}\varepsilon_m\vec{V} + \dfrac{K_\varphi}{K_P}Z_f C_f F\nabla\varphi_e & \text{Membrane} \end{cases} \tag{1b}$$

The viscosity of the gas mixture is calculated by the following equations [20]:

$$\mu_{mix} = \sum_i \frac{w_i\mu_i}{\sum_j w_j\gamma_{ij}} \tag{1c}$$

$$\gamma_{ij} = \frac{1}{\sqrt{8}}\left(1+\frac{M_i}{M_j}\right)^{-1/2}\left[1+\left(\frac{\mu_i}{\mu_j}\right)^{1/2}\left(\frac{M_j}{M_i}\right)^{1/4}\right]^2 \tag{1d}$$

Also, Stefan-Maxwell equation is employed to define the transport of multi-component gas species.

$$\nabla\cdot\left[-\rho w_i\sum_j\left(D_{ij}^{eff}\nabla x_j + (x_j - w_j)\frac{\nabla p}{p}\right) + \rho w_i u\right] = S_i \quad i=H_2O, O_2, H_2 \tag{2a}$$

The diffusion coefficient in the free space is calculated as follows [20]:

$$D_{ij} = \frac{a(T/\sqrt{T_{ci}T_{cj}})^b (P_{ci}P_{cj})^{1/3}(T_{ci}T_{cj})^{5/12}\left(\frac{1}{M_i}+\frac{1}{M_j}\right)^{1/2}}{P} \tag{2b}$$

In non-polar gases, a and b are equal to 3.640×10^{-4} and 2.334 [20]. In porous media, (i.e., gas diffusion layer, catalyst layers and membrane), it is necessary to define the effective diffusion [21]:

$$D_{ij}^{eff} = \varepsilon^{1.5}D_{ij} \tag{2c}$$

The current transport in catalyst layer and proton exchange membrane is calculated as follows [18]:

Electron transport equation:

$$\nabla\cdot(\sigma_s^{eff}\nabla\varphi_s) = -i_{v,\,total} \qquad \sigma_s^{eff} = \sigma_s\varepsilon_s^{1.5} \tag{3a}$$

Proton transport equation:

$$\nabla\cdot(\sigma_m^{eff}\nabla\phi_m) = i_{v,\,total} \qquad \sigma_m^{eff} = \sigma_m\varepsilon_m^{1.5} \tag{3b}$$

$$i_{v,\,total}\begin{cases} 0 & \text{membrane} \\ \sum_m i_{v,\,m} & \text{catalyst} \\ 0 & \text{GDL} \end{cases} \tag{3c}$$

In catalyst layer, $i_{v,m}$ (J_{an}) and J_{ca} show the anode and the cathode side, respectively. J_{ca} and J_{an} are the current densities that have been calculated based on Butler-Volmer [22].

$$\text{Anode: } J_{an} = aJ_{0,\,an}^{ref}\left(\frac{C_{H_2}}{C_{H_2}^{ref}}\right)^{0.5}\left(\frac{\alpha_{an}+\alpha_{ca}}{RT}F\eta_{an}\right) \tag{4}$$

$$\text{Catode: } J_{ca} = -aJ_{0,\,ca}^{ref}\left(\frac{C_{O_2}}{C_{O_2}^{ref}}\right)\cdot\exp\left(\frac{-\alpha_{ca}}{RT}F\eta_{ca}\right) \tag{5}$$

η_{an} and η_{ca} are over-potentials in anode and cathode, respectively, and are defined as:

$$\eta_{an} = -\varphi_m \tag{6}$$

$$\eta_{ca} = \varphi_s - \varphi_m - V_{oc} \tag{7}$$

where φ_s is the potential of the electronically conductive solid matrix (electric potential), φ_m is the electrolyte phase potential, and V_{oc} is the open-circuit potential. The open circuit potential as the function of temperature is calculated by the equation of Bernardi and Verbrugge [23].

$$V_{oc} = 0.0025T + 0.2329 \tag{8}$$

V_{oc} is the maximum of the voltage that can be delivered by the PEM fuel cell. But, the PEM fuel cell operating voltage is smaller than this value. This fact is due to over-potentials, the activation over-potential, the ohmic over-potential, and the concentration over-potential. Therefore, the PEM fuel cell operating voltage and ohmic over-potential can be calculated as [25]:

$$V_c = V_{oc} - \eta_{ca} - \eta_{an} - \eta_{ohm} - \eta_{con} \tag{9}$$

$$\eta_{ohm} = \frac{l_{mem}}{\sigma_{mem}} \tag{10}$$

and η_{con} can be expressed as [21]:

$$\eta_{con} = -B\ln\left(1-\frac{1}{I_{max}}\right) \tag{11}$$

I_{max} and B are the maximal current and coefficient dependent on the cell electrochemical characteristics. The source terms (Eq. (2a)) for O_2, H_2 and the production of water are, respectively, given by:

$$S_{H_2} = \frac{-J_{an}}{2F} \tag{12}$$

$$S_{O_2} = -\frac{J_{ca}}{4F} \tag{13}$$

$$S_{H_2O} = \frac{J_{ca}}{2F} \tag{14}$$

2. Additional Constitutive Equations

The correlation of PBI proton conductivity as electrolyte to the doping level and temperature is as follows [24]:

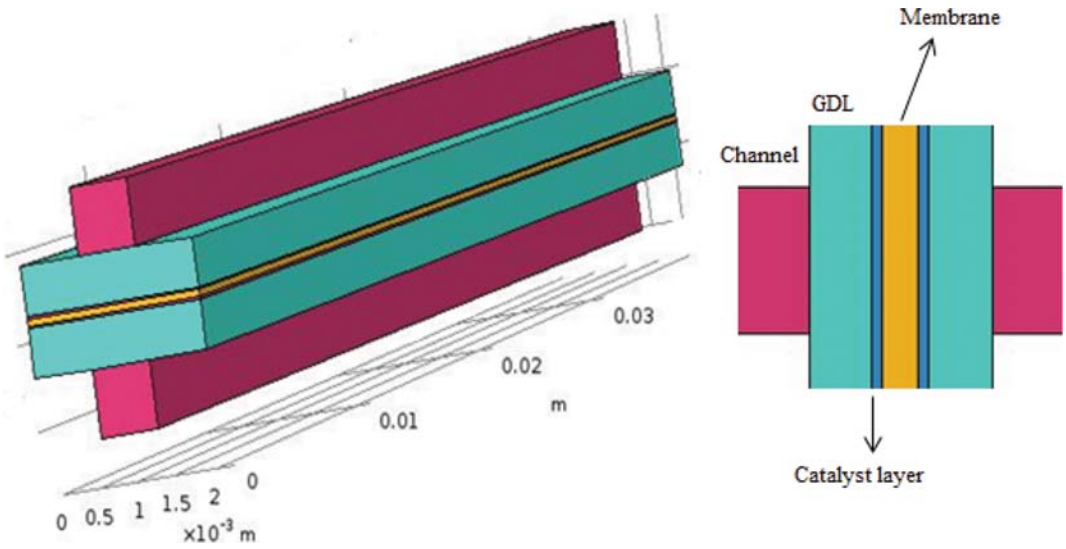

Fig. 1. The physical model for PEMFC.

$$\sigma_m = \frac{100}{T}\exp\left[8.0219 - \left(\frac{2605.3 - 70.1X}{T}\right)\right] \quad (15)$$

X is the doping level of H_3PO_4 in PBI membrane. It is a function of the acid concentration (M) at room temperature, as below [24]:

$$X = 0.012M^3 - 0.2111M^2 + 1.2363M + 0.7119 \quad (16)$$

3. Boundary Conditions

Boundary conditions are applied as:

- Zero flux condition for the walls of the cell
- No slip boundary condition for all channel walls
- Convective flux boundary conditions in channel outlet
- Stoichiometric flow rate was used to estimate the inlet concentration of the reactant gases (hydrogen and oxygen)
- Isolation of HTPEMFC from environment
- The doping level of H_3PO_4 in PBI membrane is stable and does not change with time.

4. 3D PEMFC Simulation by Using Comsol Multiphysics

Fig. 1 shows the shape of a three-dimensional fuel cell consisting of three sections: cathode, anode and membrane. The model equations related to channel, catalyst layer, GDL and membrane were solved using Comsol Multiphysics software. This software is a powerful modeling package that solves PDE systems by using finite element method (FEM). The physics of fluid flow was put into effect by introducing Navier-Stokes and Brinkman equations for the channel regions and the porous media, respectively. In simulation of the fluid flow in three sections, the calculated velocity is coupled with the chemical species transport physics and the mass transfer equations.

With solving of Maxwell-Stefan mass transfer equation, the amount of fuel transfer to the catalyst layer and the reaction on the catalyst surface was obtained. The results of mass transfer were coupled with electrochemical physics, and the current density and calculated on the basis of the Butler-Volmer equation. In each of the three sections of the fuel cell, polarization curve, concentration distribution, and velocity distribution were obtained through coupling these three physics. The model parameters are given in Table 1.

Table 1. List of parameters for high temperature PEM fuel cell modeling

Parameter	Value
Cell length (m)	0.04
Channel height (m)	7.5×10^{-4}
Channel width (m)	7.5×10^{-4}
GDL width	550×10^{-6}
Porous electrode thickness (m)	25×10^{-6}
Membrane thickness (m)	75×10^{-6}
GDL porosity	0.5
GDL electric conductivity (S/m)	687.5
Inlet H_2 mass fraction	0.99
Inlet H_2O mass fraction	0.002
Inlet O_2 mass fraction	0.208
Proton conductivity of electrolyte (S/m)	10
Cell temperature (K)	433
Reference pressure (Pa)	120,000
Cell voltage (V)	0.6
$J_{0,an}^{ref}$ (A/m^3)	1×10^9
$J_{0,ca}^{ref}$ (A/m^3)	3×10^5 exp(0.014189(T−353 [K])

DESIGN OF EXPERIMENT

For more detailed analysis of the input variables effect on the fuel cell performance, design of experiments (DOE) is necessary. DOE is a systematic method to obtain the relationship of variables affecting of process inputs with the output response of the process. It enables extracting much information from a limited number of test cases. For example, for a four-design factors case, a three-level full factorial method will require 81 tests. However, when using the three-level Box-Behnken experimental design, 24 tests are required

Table 2. Box-Behnken design matrix with four independent variables expressed in coded and real terms

Run	Air velocity x_1 (m/s)		Hydrogen velocity x_2 (m/s)		Temperature x_4 (K)		Acid doping level x_3 (mol of PA per PBI repeat unit)		Average current density (A/cm^2)
Number	Coded	Uncoded	Coded	Uncoded	Coded	Uncoded	Coded	Uncoded	
1	−1	0.5	0	0.15	0	363	−1	2	1.092612
2	−1	0.5	−1	0.1	0	363	0	9	1.254663
3	−1	0.5	+1	0.2	0	363	0	9	1.254663
4	−1	0.5	0	0.15	−1	298	0	9	0.546327
5	−1	0.5	0	0.15	+1	428	0	9	1.975036
6	−1	0.5	0	0.15	0	363	+1	16	4.207457
7	0	0.9	0	0.15	−1	298	−1	2	0.452958
8	0	0.9	0	0.15	+1	428	−1	2	1.853534
9	0	0.9	−1	0.1	0	363	−1	2	1.105118
10	0	0.9	+1	0.2	0	363	−1	2	1.105128
11	0	0.9	−1	0.1	+1	428	0	2	1.852954
12	0	0.9	−1	0.1	−1	298	0	2	0.452947
13	0	0.9	+1	0.2	+1	428	0	2	1.853554
14	0	0.9	0	0.15	0	363	0	2	1.104892
15	0	0.9	0	0.15	0	363	0	2	1.104892
16	0	0.9	0	0.15	0	363	0	2	1.104892
17	0	0.9	+1	0.2	−1	298	0	2	0.452952
18	0	0.9	0	0.15	0	363	0	2	1.104892
19	0	0.9	0	0.15	0	363	0	2	1.104892
20	0	0.9	−1	0.1	0	363	+1	16	4.304981
21	0	0.9	0	0.15	−1	298	+1	16	3.515106
22	0	0.9	+1	0.2	0	363	+1	16	4.204911
23	0	0.9	0	0.15	+1	428	+1	16	4.570751
24	+1	1.3	0	0.15	0	363	−1	2	1.107723
25	+1	1.3	0	0.15	+1	428	0	9	2.086286
26	+1	1.3	−1	0.1	0	363	0	9	1.278497
27	+1	1.3	0	0.15	−1	298	0	9	0.549399
28	+1	1.3	+1	0.2	0	363	0	9	1.277232
29	+1	1.3	0	0.15	0	363	+1	16	4.583851

[25]. RSM has been successfully used to optimize various processes [26-28]. The number of tests required for development of a Box-Behnken matrix is defined according to the following equation:

$$N=2k(k-1)+C_0 \tag{17}$$

where k is the number of factors and C_0 is the number of repetitions of the center point. This is ideal for CFD simulation cases, because a simulation can run on for hours or even days. Using the DOE technique, a set of numerical experiments or simulations is performed for a permitted set of design points to construct a measured response level in the design space, i.e., a function $\eta(x_1, x_2, \ldots, x_n)$, where x_1, x_2, x_3, …, x_n are variables affecting the process and are considered in design within a certain range. When a second-order polynomial equation is used, the response surface equation is written as follows:

$$f=a_0+\sum_{j=1}^{n}a_j x_j+\sum_{j=1}^{n}a_{jj}x_j^2+\sum\sum_{i\neq j}^{n}a_{ij}x_i x_j \tag{18}$$

where a_{ij} is the unknown coefficient of the polynomial equation that is determined using calculated values of the measured quantity for the prescribed set of design points, and f refers to the quadratic model. Design Expert software was used in this study. Four operating parameters including, hydrogen gas velocity, air velocity, operating temperature and amount of acid-doping in membrane, were applied. The level of each parameter is shown in Table 2. The objective function is the sum of the current density in the investigated voltage range, which is calculated from the following equation:

$$f=\sum_{V=0.4}^{V=0.9} I[A/m^2] \tag{19}$$

To test the significance of response surface model, R^2_{adj} is investigated, and we need to verify that R^2_{adj} has a value close to 1, and the closer the R^2 is to one, the more the fitted model's ability in describing the response variations as a function of the independent variables [29].

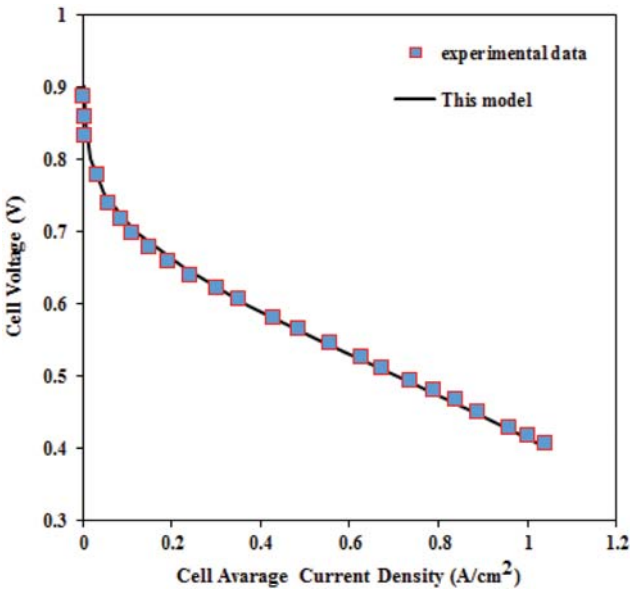

Fig. 2. Comparison between simulation and experimental data.

RESULTS AND DISCUSSION

1. Model Validation

In this section, for mathematical model validation, the simulation results are compared with experimental data [30] and comparison is shown in Fig. 2. Experimental data relates to single-cell fuel cell at 160 °C, in which PBI polymer is used as electrolyte. The continuous black lines represent the results of the model, and the red dots represent the experimental data. As can be seen from the figure, the model strongly predicts the experimental data. The maximum error in this fit was 3%. Many studies have compared polarization curves as obtained experimentally and numerically. A fairly strong agreement is found between experimental and numerical data in these studies. However, sensitivity analyses, the effect of operating parameters and their interaction have not been properly explored.

2. Analyses of Variance (ANOVA)

Using the Comsol Multiphysics, the response function was calculated in all design points according to Eq. (19). According to the normality plot shown in Fig. 3, it could be verified whether the results are normally distributed and the remaining normality plot is a straight line that does not show any abnormalities.

Using the regression analysis on the design matrix and the obtained response, the second-order polynomial equation in the encoded functions was obtained here:

$$\begin{aligned} f = {} & +1.10489+0.031144x_1+0.00648125x_2+0.6852x_3 \\ & +1.55583x_4+0.044307x_1x_2+0.027044x_1x_3+0.09032x_1x_4 \\ & +0.00014875x_2x_3-0.025x_2x_4-0.086233x_3x_4+0.01282x_1^2 \\ & +0.0266x_2^2+0.019441x_3^2+1.51223x_4^2 \end{aligned} \quad (20)$$

Where f is the total predicted current density, x_1, x_2, x_3 and x_4 coded terms for the four independent test variables. The highest constant coefficient in Eq. (20) is related to the factors x_3 (T) and x_4 (PA doping level), which are the most important factors affecting the response. Considering that PA_{dop} and T have a direct relationship with the proton conductivity of the membrane, the increase in these two factors leads to a significant increase in the proton conductivity of the membrane and subsequently improves the fuel cell performance. Altan has reported that analysis of variance is essential to test the importance of the model [31]. Also, the effect of independent param-

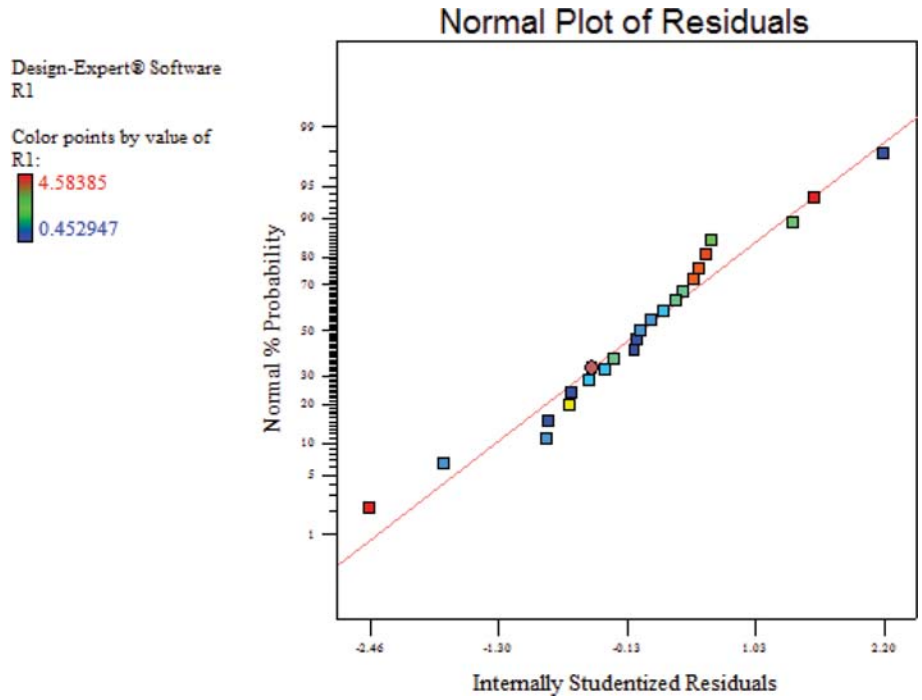

Fig. 3. Normality plot.

Table 3. ANOVA Table for the prediction of purpose function

Source	Sum of squares	df	Mean square	F value	P-value Prob>F
Model	50.27	14	3.59	339.66	<0.0001
A-A	0.025	1	0.025	2.40	0.1434
B-B	8.454E-04	1	8.454E-04	0.080	0.7815
C-C	5.63	1	5.63	532.90	<0.0001
D-D	29.05	1	29.05	2747.48	<0.0001
AB	4.001E-07	1	4.001E-07	3.784E-005	0.9952
AC	2.926E-03	1	2.926E-03	0.28	0.6071
AD	0.033	1	0.033	3.09	0.1008
BC	8.851E-08	1	8.851E-08	8.371E-006	0.9977
BD	2.504E-03	1	2.504E-03	0.24	0.6340
CD	0.030	1	0.03	2.81	0.1157
A^2	0.13	1	0.13	12.63	0.0032
B^2	0.011	1	0.011	1.06	0.3217
C^2	9.345E-04	1	9.345E-04	0.088	0.7706
D^2	14.69	1	14.69	1389.29	<0.0001
Residual		0.15	14	0.011	
Lack of fit		0.15	10	0.015	
Pure error		0.00	4	0.000	
Cor total		50.42	28		

eters on the response can be evaluated through the analysis of the RSM contour plots. Analysis of variance (ANOVA) was used to test the second-order polynomial equation fitting for the simulation results given in Table 3.

The significance of the model is evaluated on the basis of the value of the two parameters F-value and P-value. The larger the F-value and the smaller the P-value, the higher the significance of the model. Furthermore, the calculated F value was found to be higher than the tabulated F value at the 5% level, indicating that the computed Fisher's variance ratio was large enough at this level [32]. Since $F_{cal}>F_{tab}$ (47.31>3.68), it was concluded on the basis of Fisher's F-test, with 95% certainty that the regression model explained a significant amount of the variation in the dependent variable. To check the goodness of fit of the model and the importance of the model, the determination coefficient and adjusted determination coefficient were used. In this case, the value of the determination coefficient shows that only 1.3% of the total variables were not explained by the regression model. Moreover, the closer the value of the adjusted determination coefficient to 1 shows the high significance of the model, which is reported in similar studies [33-35]. Liu et al. [33] reported that the R_a^2 corrects the R^2 value for the sample size and the number of terms in the model. The results showed that there are many terms in the model and the sample size is small. In this analysis, the R_a^2 obtained was very close to the R^2 value. In addition, the very high and close to one values of the correlation coefficient (R=0.9919) represents a great correlation between predicted values and simulation results. Yetilmezsoy et al. [32] reported that the main and interactive effects of the two factors on the response could be investigated using the three-dimensional 3D RSM plots as a function of two factors, where the remaining factors are kept at a constant level. There are four independent variables in this model, two variables are kept constant in each plot. Fig. 4 shows the response surface diagrams as the functions of two variables at the center level of other variables. In addition, the effect of independent variables on the response can be more easily obtained using the 3D response surface plots and their corresponding contour plots. Figs. 4 and 5 show three-dimensional and two-dimensional plots as functions of two variables at the center level of other variables. It is reported that the nonlinear nature of the 3D RSM and the respective contour plots can indicate the importance of the interaction effect of the two factors on the response.

As shown in Fig. 4 and Fig. 5, the x_1x_2, x_3x_4, x_1x_4, x_2x_4 interactions have a significant effect on the response. In Fig. 4, the nonlinear Figs. 4(a), (c), (e), and (f) were investigated. It can be concluded that the interactions examined in these figures are effective on the response. In the interactions x_3x_4, x_1x_4, x_2x_4, there are two independent factors, including T and PA_{dop}. Due to the importance of these two factors on the proton conductivity of the membrane in high temperature fuel cell, their interaction is also important. Fig. 4(f) shows the effect of interactions of two T and PA factors on the response. As shown in in the figure, the response variable increases with simultaneous increase of these two factors. Additionally, Fig. 5 shows that the Figs. 5(a), (c), (e), and (f) are non-linear, confirming the results obtained from Fig. 4. Moreover, it is obvious that the most important interaction is related to two factors of T and PA. According to Eq. (15), the proton conductivity of the membrane is a direct function of the acid doping level and operating temperature, i.e., increases in both of these parameters leads to an increase in proton conductivity of the membrane. The effect of each parameter on the response can be evaluated based on the ANOVA.

As can be seen in Table 3, the most important factors affecting the response are x_3 and x_4, the F value of which was 532.90 and 2747.48, respectively. That is, the acid doping level of the membrane exerts a greater effect on current density changes, because it causes a significant increase in the proton conductivity of the membrane. It is also seen from the regression equation that the constant coefficient of the factor x_4 is greater than the constant coefficient x_3. This confirms that the doping acid level is more effective than the operating temperature. Acid doping level of the membrane has a greater effect on response, compared to operating temperature. In the PBI membrane, the doping level is a major cause of increased proton conductivity of the membrane, so when the PA_{dop} is greater than 2, the additional free acid content within the membrane is increased, which facilitates the transport of the proton across the membrane. The acid doping level of the membrane in this analysis was in the range of 2 to 16 mol of PA per PBI unit, which is greater than 2. Therefore, the key controller of proton conductivity of the membrane is the excess free acid. It is observed in all three-dimensional and two-dimensional plots (Fig. 4 and Fig. 5) that for the acid doping level of membrane above the center, the response function is greater. In addition, with increasing temperature, as the activation energy decreases for proton transfer, the proton conductivity of the membrane increases, which leads in turn to an increase in the current density. According to the results, the highest response amount was obtained at the highest temperature and highest acid-doping level of the membrane (PA_{dop}= 16 and T=160 °C).

Also, the results of analysis of variance show that the indepen-

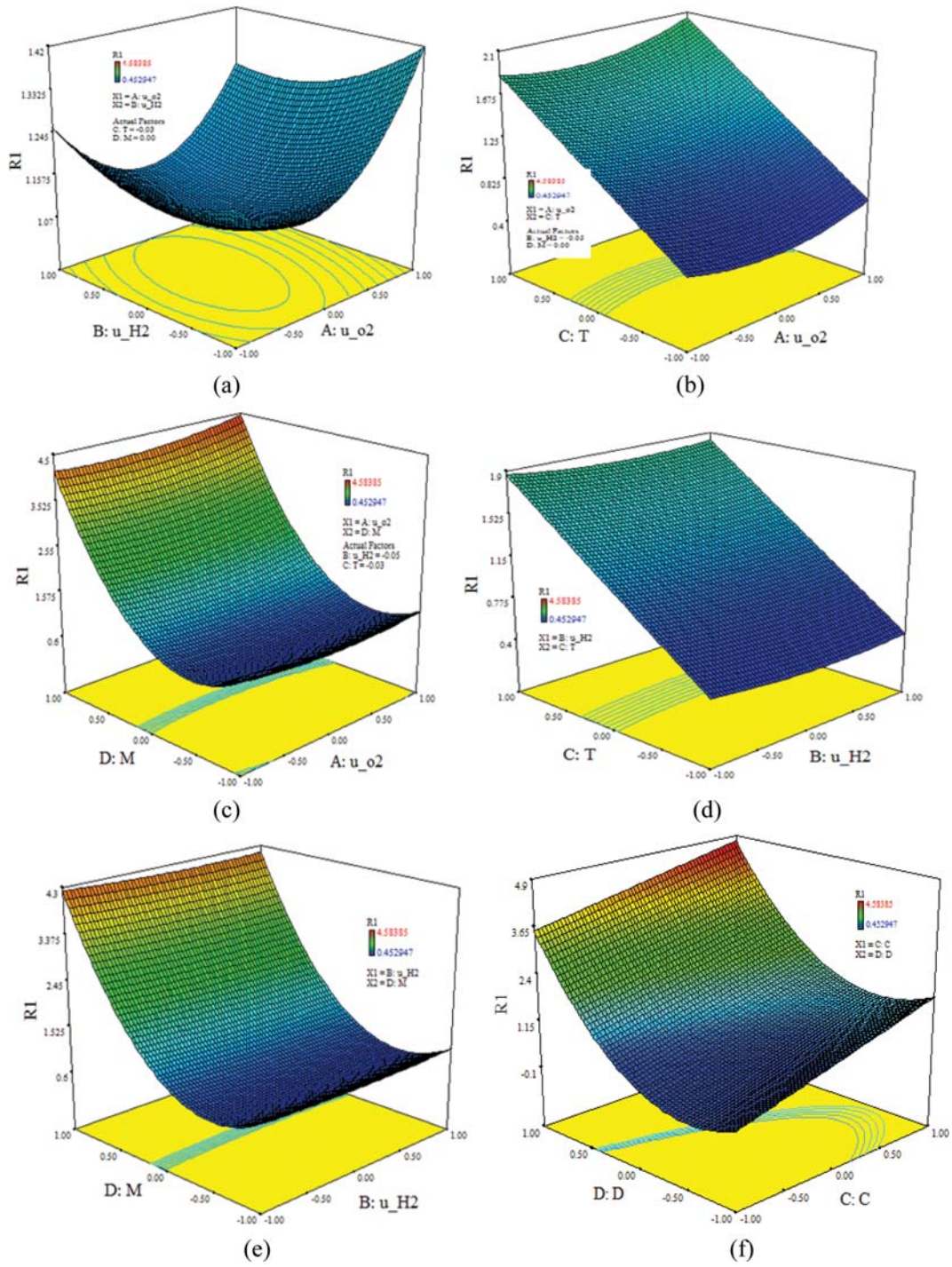

Fig. 4. Response surface diagrams showing the effects of the mutual interactions between two independent variables.

dent variable x_2 has not a significant effect on the response function because its corresponding F value is very small. The hydrogen gas with 99% purity entered the channel, so increasing gas velocity does not significantly increase the transfer of hydrogen gas to the catalyst layer; therefore, the effect of this variable can be ignored.

Also, factor x_1 is considered ineffective in comparison with factors x_3 and x_4, but when the effect of factor on the response function is separately investigated, it is considered to be an important factor affecting the performance of fuel cells because the oxygen concentration in the cathode channel decreases due to the electrochemical reaction. Therefore, increasing the air velocity inside the cathode channel results in a greater amount of oxygen penetrating into the cathode catalyst layer, resulting in increased current density.

Similarly, the RSM method was used to determine the optimal conditions [17]. Fig. 6 shows the voltage diagram in terms of cur-

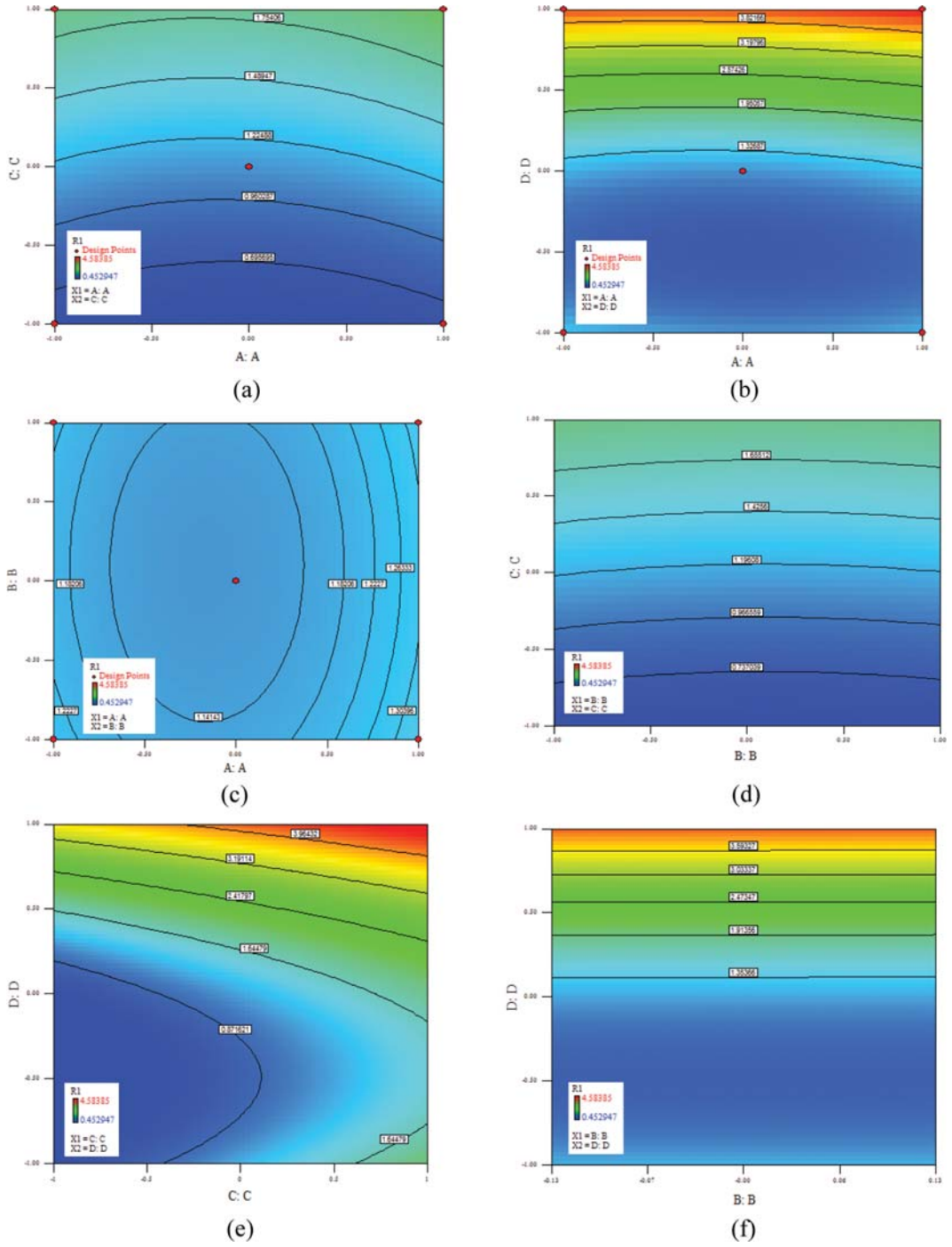

Fig. 5. Contour plots exhibiting the interactive effects between two independent variables (other variables were held at their respective center levels).

rent density. The plots are related to design points of runs 26, 21, 3, 16 and 8. On the runs 8, 21, and 16, two factors x_3 and x_4 change, and factors x_1 and x_2 were kept constant at the center point. Also, on the runs 3 and 26, factors x_3 and x_4 were kept constant at the center point, and the effect of the variations of factors x_1 and x_2 on fuel cell performance was investigated. As seen from the figure, the performance of the fuel cell increases significantly with an increase in two factors x_3 and x_4, but with an increase in two factors x_1 and x_2, fuel cell performance has not changed significantly, which confirms the reported results from the sensitivity analysis using the Design Expert software.

Increasing the transfer of fuel to the catalyst layer by increasing the velocity of the reaction gases and increasing the proton transfer from the membrane through increasing the proton conductivity by increasing the temperature and PA can improve the performance of the fuel cell. However, since the reaction of each mole of

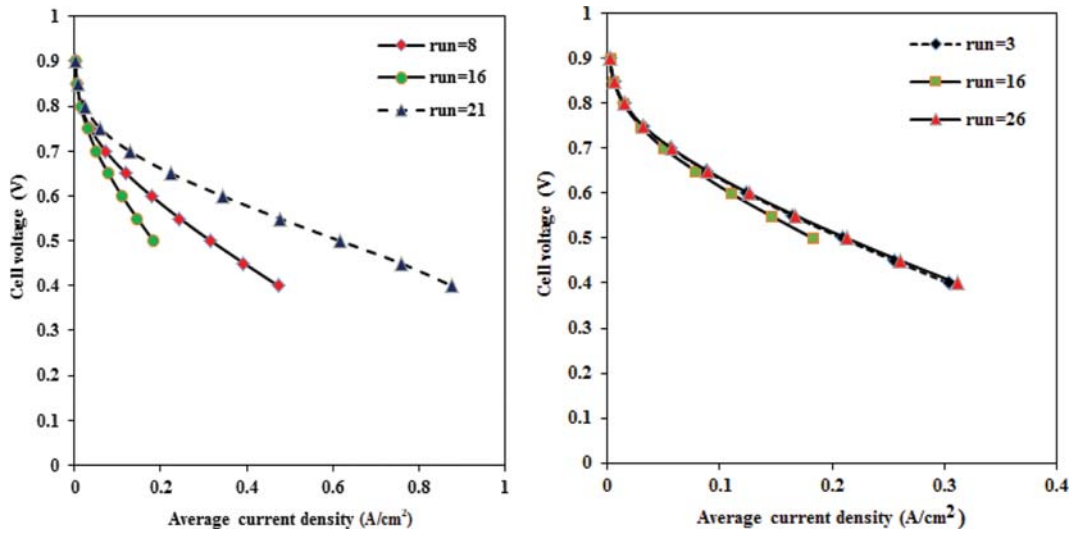

Fig. 6. Simulated polarization curve of a single HT-PEMFC obtained for run=3, 8, 16, 21 and 26.

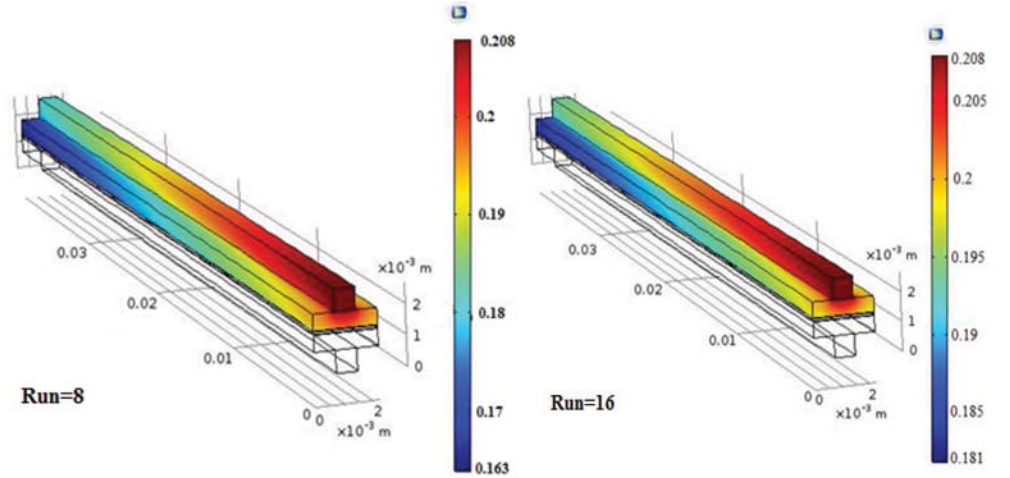

(a) Oxygen mole fraction profile

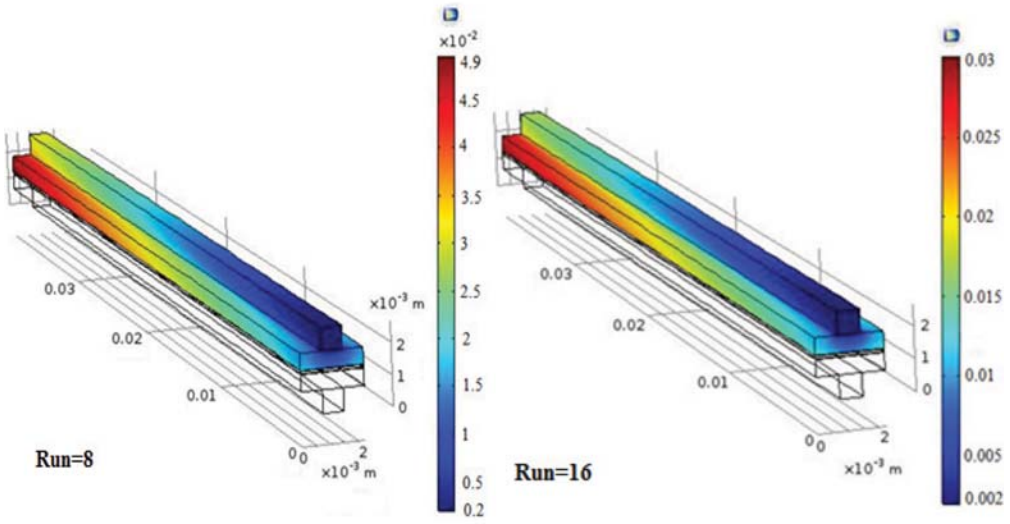

(b) Water mole fraction profile

Fig. 7. Mole fraction profiles along cathode gas channel predicted for V=0.6 V.

hydrogen produces two protons, therefore, the proton conductivity of the membrane is more important than gas velocity.

3. Channel Mole Fraction Profiles of Reactants and Product along a Single Channel

The mole fraction profile in the cathode section for oxygen and water is shown in Fig. 7(a) and 7(b), respectively (runs 16 and 8). On run 8, factors x_1 and x_2 are selected at the center point, and factors x_3 and x_4 are at their low level. On run 21, the factor x_3 is at its low level and the factor x_4 is high level. The rest of the modeling conditions are the same. As shown in Fig. 7(a), the oxygen mole fraction decreases along the channel, because oxygen is consumed through the electrochemistry reaction and water is produced. On run 8, the mole fraction of oxygen input to the cathode channel is 0.208 and it decreases to 0.163 at the outlet. On run 16, the mole fraction of oxygen input to the channel is 0.208 and it decreases to 0.181 at the outlet. Therefore, under conditions in run 8, a greater amount of oxygen has been involved in the reaction and converted to water. Also, according to Fig. 7(b), the mole fraction of water at the output of the run 8 is greater than that of the run 16. In fact, when the reaction occurs, more water is produced, resulting in a higher concentration of water along the channel. This observation confirms that PA_{dop} is the most effective factor on the response.

CONCLUSION

High-temperature fuel cell sensitivity analysis was performed using Comsol Multiphysics software and Design Expert software. The results of the model were validated with experimental data. The experimental design was carried out using the Box-Behnken method, and the effect of four independent factors including air and hydrogen velocity, operating temperature and acid doping level of membrane on the fuel cell performance was investigated. The results showed that the two factors of temperature and acid doping level of membrane are the most effective factors on fuel cell performance, and since the acid doping level of membrane has a significant effect on proton conductivity of the membrane, with the increase in the acid doping level of membrane, the fuel cell performance increases significantly. Interaction effects of independent factors were also examined and the results showed that the interactions of factors x_1x_2, x_1x_4, x_2x_4 and x_3x_4 affect the response, but compared with factor x_4, the interactions of these factors were insignificant. As a result, the most important factor that causes a significant change in the performance of the fuel cell is factor x_4, and if factor x_4 is considered constant, factor x_3 is the factor affecting the response. When the temperature and acid doping level are kept constant, factor x_1, i.e., the air velocity in the cathode channel, is the factor affecting the response.

NOMENCLATURE

a : effective catalyst area per unit volume [m^2/m^3]
act : water activation
C : concentration
D : mass diffusivity [m^2/s]
F : Faraday's number [C/mol]
I : current density [A/m^2]
J : transfer current [A/m^3]
K : permeability [m^2]
L : thickness
R : universal gas constant [J/(mol·K)]
Re : Reynolds number
S : source term
T : temperature [K]
V : cell potential [V]
X : mole fraction of species
z : site charge number

Greek

α : transfer coefficient
λ : water content
σ : protonic conductivity [$\Omega^{-1}m^{-1}$]
ε : porosity
μ : dynamic viscosity [Pa s]
ρ : density [kg/m^3]
η : over potential [V]
φ : phase potential [V]

Subscripts

an : anode
ca : cathode
C : catalyst layer
GDL : gas diffusion layer
eff : effective
i : species (H_2, O_2, H_2O)
ref : reference

REFERENCES

1. Y. Devrim, S. Erkan, N. Bac and I. Eroğlu, *Int. J. Hydrogen Energy*, **34**, 3467 (2009).
2. Q. Li, R. He, J. O. Jensen and N. J. Bjerrum, *Chem. Mater.*, **15**, 4896 (2003).
3. D. Cheddie and N. Munroe, *J. Power Sources*, **156**, 414 (2006).
4. Z. Qi, C. He and A. Kaufman, *J. Power Sources*, **111**, 239 (2002).
5. O. Kongstein, T. Berning, B. Børresen, F. Seland and R. Tunold, *Energy*, **32**, 418 (2007).
6. D. Weng, J. Wainright, U. Landau and R. Savinell, *J. Electrochem. Soc.*, **143**, 1260 (1996).
7. D. Ergun, Y. Devrim, N. Bac and I. Eroglu, *J. Appl. Polym. Sci.*, 124 (2012).
8. S. Gant, A. Kelsey, K. McNally, H. Witlox and M. Bilio, *J. of Loss Prevention in the Process Industries*, **26**, 792 (2013).
9. M. Haghayegh, M. H. Eikani and S. Rowshanzamir, *Int. J. Hydrogen Energy*, **42**, 21944 (2017).
10. Y.-J. Sohn, S.-D. Yim, G.-G. Park, M. Kim, S.-W. Cha and K. Kim, *Int. J. Hydrogen Energy*, **42**, 13226 (2017).
11. R. B. Lakshmi, N. Harikrishnan and A. V. Juliet, *Appl. Surf. Sci.*, **418**, 99 (2017).
12. S. Li and B. Sundén, *Int. J. Hydrogen Energy*, **42**, 27323 (2017).
13. R. Bradfield, G. Cairns and G. Wright, *Technological Forecasting and Social Change*, **100**, 44 (2015).

14. S.-J. Wang and S.-Y. Lee, *Computational Statistics & Data Analysis*, **23**, 239 (1996).
15. M. Hadzima-Nyarko, E. K. Nyarko and D. Morić, *Expert Systems with Applications*, **38**, 13405 (2011).
16. E. Zio, N. Pedroni and M. Carlo, *Reliability Engineering & System Safety*, **107**, 90 (2012).
17. J. Mousavi and M. Parvini, *Int. J. Hydrogen Energy*, **41**, 5188 (2016).
18. P. Chippar and H. Ju, *Solid State Ionics*, **225**, 30 (2012).
19. J. Lobato, P. Cañizares, M. A. Rodrigo, F. J. Pinar, E. Mena and D. Úbeda, *Int. J. Hydrogen Energy*, **35**, 5510 (2010).
20. R. O'hayre, S.-W. Cha, F. B. Prinz and W. Colella, Fuel cell fundamentals, Wiley (2016).
21. T. E. Springer and S. Gottesfeld, Pseudo homogeneous catalyst layer model for polymer electrolyte fuel cell, Los Alamos National Lab., NM (United States) (1991).
22. D. Song, Q. Wang, Z. Liu, T. Navessin and S. Holdcroft, *Electrochim. Acta*, **50**, 731 (2004).
23. D. M. Bernardi and M. W. Verbrugge, *J. Electrochem. Soc.*, **139**, 2477 (1992).
24. D. F. Cheddie and N. D. Munroe, *Int. J. Hydrogen Energy*, **32**, 832 (2007).
25. R. H. Myers, D. C. Montgomery, G. G. Vining, C. M. Borror and S. M. Kowalski, *J. Quality Technol.*, **36**, 53 (2004).
26. M. Khajeh, *J. Supercrit. Fluids*, **55**, 944 (2011).
27. A. Kanaris, A. Mouza and S. Paras, *Int. J. Thermal Sci.*, **48**, 1184 (2009).
28. J. G. Carton and A.-G. Olabi, *Energy*, **35**, 2796 (2010).
29. H.-M. Kim and K.-Y. Kim, *Int. J. Heat and Mass Transfer*, **47**, 5159 (2004).
30. B. Sezgin, D. G. Caglayan, Y. Devrim, T. Steenberg and I. Eroglu, *Int. J. Hydrogen Energy*, **41**, 10001 (2016).
31. M. Altan, *Mater. Design*, **31**, 599 (2010).
32. K. Yetilmezsoy, S. Demirel and R. J. Vanderbei, *J. Hazard. Mater.*, **171**, 551 (2009).
33. H.-L. Liu, Y.-W. Lan and Y.-C. Cheng, *Process Biochem.*, **39**, 1953 (2004).
34. K. Adinarayana and P. Ellaiah, *J. Pharm. Pharm. Sci.*, **5**, 272 (2002).
35. D. Wu, J. Zhou and Y. Li, *Chem. Eng. Sci.*, **64**, 198 (2009).